Cancer Cell
Article

Translational Activation of Snail1 and Other Developmentally Regulated Transcription Factors by YB-1 Promotes an Epithelial-Mesenchymal Transition

Valentina Evdokimova,[1,2,7,*] Cristina Tognon,[3,7] Tony Ng,[3] Peter Ruzanov,[4] Natalya Melnyk,[3] Dieter Fink,[3] Alexey Sorokin,[2] Lev P. Ovchinnikov,[2] Elai Davicioni,[5] Timothy J. Triche,[6] and Poul H.B. Sorensen[1,3,*]
[1]Department of Molecular Oncology, British Columbia Cancer Research Centre, Vancouver, BC V5Z 1L3, Canada
[2]Institute of Protein Research, Pushchino, Moscow Region 142290, Russia
[3]Department of Pathology
[4]Michael Smith Laboratories
University of British Columbia, Vancouver, BC V6T 1Z4, Canada
[5]Genome Diagnostics, Inc., Pasadena, CA 91101, USA
[6]Department of Pathology and Laboratory Medicine, Children's Hospital Los Angeles, Los Angeles, CA 90027, USA
[7]These authors contributed equally to this work
*Correspondence: v.evdokimova@gmail.com (V.E.), psor@interchange.ubc.ca (P.H.B.S.)
DOI 10.1016/j.ccr.2009.03.017

SUMMARY

Increased expression of the transcription/translation regulatory protein Y-box binding protein-1 (YB-1) is associated with cancer aggressiveness, particularly in breast carcinoma. Here we establish that YB-1 levels are elevated in invasive breast cancer cells and correlate with reduced expression of E-cadherin and poor patient survival. Enforced expression of YB-1 in noninvasive breast epithelial cells induced an epithelial-mesenchymal transition (EMT) accompanied by enhanced metastatic potential and reduced proliferation rates. YB-1 directly activates cap-independent translation of messenger RNAs encoding Snail1 and other transcription factors implicated in downregulation of epithelial and growth-related genes and activation of mesenchymal genes. Hence, translational regulation by YB-1 is a restriction point enabling coordinated expression of a network of EMT-inducing transcription factors, likely acting together to promote metastatic spread.

INTRODUCTION

Mammalian Y-box binding protein-1 (YB-1) is a member of the DNA/RNA-binding family of proteins with an evolutionarily conserved cold-shock domain (CSD). Both bacterial and mammalian cold-shock domain proteins are ubiquitously expressed and involved in fundamental processes such as DNA repair, mRNA transcription, splicing, translation, and stabilization (Evdokimova and Ovchinnikov, 1999; Kohno et al., 2003). Consistent with its essential biological functions, targeted disruption of *YB-1* in mice causes severe developmental defects and embryonic lethality (Lu et al., 2005).

Numerous studies point to a role for YB-1 in malignant transformation, with evidence for both oncogenic and tumor-suppressive functions. A prooncogenic role for YB-1 is suggested by its higher expression in actively proliferating tissues and multiple human malignancies, as well its ability to activate transcription of proliferation-related genes through binding to the Y-box promoter elements of the latter (Kohno et al., 2003). However, only a few reports have directly addressed the biological role of YB-1 in tumorigenesis. Bergmann et al. (2005) found that elevated YB-1 expression in mammary glands caused chromosomal instability and induced invasive breast carcinomas in lactating transgenic mice. Another study demonstrated that in vitro YB-1

SIGNIFICANCE

Dissemination of malignant cells during breast cancer progression is hypothesized to occur through the acquisition of a migratory mesenchymal-like phenotype. Such cells may then remain quiescent only to resume their growth after years of dormancy. We demonstrate that increased YB-1 expression combined with sustained Ras-ERK activation induces epithelial dedifferentiation and metastatic ability, while simultaneously inhibiting tumor growth. YB-1-overexpressing breast cancer cells therefore closely recapitulate the early steps of metastatic spread and acquired dormancy and are likely to be insensitive to conventional therapies directed at eradicating dividing cells. Our findings argue against direct targeting of YB-1 as this may reactivate proliferation of dormant metastatic cells. Instead, we propose that inactivating potential downstream effectors of YB-1 may be a better therapeutic strategy.

overexpression in MCF-7 breast carcinoma cells enhances their proliferation and soft agar colony formation (Sutherland et al., 2005). These protumorigenic activities are proposed to involve nuclear localization and transcriptional activation by YB-1.

In contrast, cytosolic YB-1 exhibits potent tumor-suppressive activity (Bader and Vogt, 2007). In normal mouse and human tissues as well as in cultured cells, YB-1 predominantly localizes to the cytoplasm where it is found in complexes with translationally inactive mRNAs (Evdokimova and Ovchinnikov, 1999). This has led to the notion that the tumor suppressor function of YB-1 involves translational silencing of progrowth transcripts, which are less competitive in translation initiation due to their extended, highly structured 5′UTRs (Bader and Vogt, 2005; Evdokimova et al., 2006a). Using a microarray approach, we previously identified diverse growth-related mRNAs that were silenced through specific binding to YB-1 in K-Ras-transformed NIH 3T3 cells (Evdokimova et al., 2006b). Translational silencing by YB-1 may arise from its ability to bind in close proximity to the 5′ mRNA cap structure and displace the eIF4E-driven translation initiation complex from mRNAs (Bader and Vogt, 2005; Evdokimova et al., 2006b, 2001). YB-1's ability to repress cap-dependent translation and tumor growth can be disabled by AKT-mediated phosphorylation (Bader and Vogt, 2007; Evdokimova et al., 2006b). Thus elevated PI3K-AKT signaling is predicted to reverse the inhibitory effects of YB-1. Moreover, AKT activation may induce the progrowth activities of YB-1 by triggering its nuclear translocation (Sutherland et al., 2005). Binding of key growth-related mRNAs in the cytoplasm by YB-1 may protect these transcripts from degradation under conditions unfavorable for proliferation, allowing for their rapid deployment through translation in response to proliferative stimuli without the need for transcriptional activation (Evdokimova et al., 2006a). In this study we investigated the effects of YB-1 on breast cancer progression to further explore the role of cytosolic YB-1 in oncogenesis.

RESULTS

YB-1 Promotes an Epithelial-Mesenchymal Transition and Reduces Proliferation of MCF10AT Breast Epithelial Cells

To address the potential contribution of YB-1 to breast tumorigenesis, HA-tagged YB-1 was ectopically expressed in immortalized benign MCF10A human mammary epithelial cells or their premalignant MCF10AT subclone. The latter is derived by transformation with oncogenic H-Ras and subsequent passaging through mouse xenografts. This model closely recapitulates the histological characteristics of mammary hyperproliferative disease and its ability to progress to carcinoma in situ and invasive cancers (Dawson et al., 1996). Parental MCF10A cells exhibit a cuboidal, cobblestone morphology in monolayer cultures, with tight cell-cell contacts characteristic of normal mammary epithelial cells (Debnath et al., 2003). This morphology was observed for both vector alone (MCF10A and MCF10AT) and MCF10A-YB-1 cell lines (Figure 1A, top row). Surprisingly, however, ectopic expression of YB-1 in MCF10AT cells at levels that are ~2-fold higher than endogenous YB-1 (see Figure 1B) led to loss of cell-cell contacts and the emergence of a spindle-shaped, fibroblast-like morphology. MCF10AT-YB-1 cells formed cord-like networks of cells with extremely long membrane extensions resembling filopodia. This was accompanied by virtually complete loss of epithelial E-cadherin and the tight junction protein ZO-1, and reduced expression of other epithelial markers including cytokeratin 18 (CK18) and mucin 1 (MUC1) (Figures 1A and 1B and Figure S1A available online). Instead, these cells expressed mesenchymal N-cadherin and many proteins characteristic of basal/myoepithelial or even progenitor-like cell lineages, such as fibronectin, vimentin, α-smooth muscle actin (SMA), CK14, and p63 (Figures 1B and Figure S1A). These alterations are characteristic of cells that have undergone an epithelial-mesenchymal transition (EMT), a process whereby epithelial cells lose polarity, cell-cell contacts, and cytoskeletal integrity and acquire metastatic ability (Thiery and Sleeman, 2006). Similar results were obtained in YB-1-overexpressing H-Ras-transformed EpH4 mouse mammary epithelial cells as well as in cervical and prostate carcinoma cells (Figures S1B–S1E), indicating that elevation of YB-1 levels may enhance mesenchymal properties in a broad range of human carcinomas.

In addition, MCF10AT-YB-1 cells exhibit reduced expression of certain G1/S and mitotic cyclins (cyclins A2, B1, D1, D3, and E1; Figure 1C) and significantly lower proliferation rates (Figure 1D). In contrast to MCF10AT-MSCV cells, which proliferated and maintained high expression levels of cyclins even under serum starvation, MCF10AT-YB-1 cells failed to reenter S phase after serum starvation (Figures 1C and 1E). Therefore, YB-1 limits the ability of MCF10AT cells to proliferate, especially under conditions where nutrients and growth factors are limited.

YB-1 Disrupts Mammary Acinar Architecture and Enhances Migration of MCF10AT Cells

To gain further insights into the potential role of YB-1 in malignant progression, we analyzed the effects of ectopic YB-1 expression on mammary acinar morphogenesis. MCF10A cells cultured on reconstituted laminin-rich 3D basement membranes (Matrigel) are known to form growth-arrested acinar-like spheroids comprised of a single layer of polarized epithelial cells surrounding a hollow lumen. These structures closely recapitulate the architecture of normal mammary glands (Debnath and Brugge, 2005; Nelson and Bissell, 2005). As expected, both MCF10A-MSCV and MCF10A-YB-1 cells formed acinar structures with hollow lumens that reached maximal size by day 5 in culture, whereas MCF10AT-MSCV cells formed somewhat larger acini with filled lumens (Figure 2A and data not shown). In striking contrast, MCF10AT-YB-1 cells were organized into networks of loosely bound spindle-shaped cells that formed elongated invasively growing cords (Figure 2A). These cord-like slow-growing structures were evident by day 1 and continued to expand until day 10, despite a lower percentage of mitotic cells and reduced expression of cyclins D1 and D3 (Figures 2A and 3C). Examination of epithelial and mesenchymal markers in 3D cultures by confocal microscopy confirmed that, similar to monolayer cultures, MCF10AT-YB-1 cells expressed exclusively N-cadherin, in contrast to the other cell lines positive for E-cadherin (Figure 2B). Notably, HA-tagged as well as endogenous YB-1 proteins were detected predominantly in the cytosol (Figure 2B and Figure S2A), consistent with our hypothesis that YB-1-mediated effects are mainly due to its cytoplasmic activities. Further support for this was obtained by

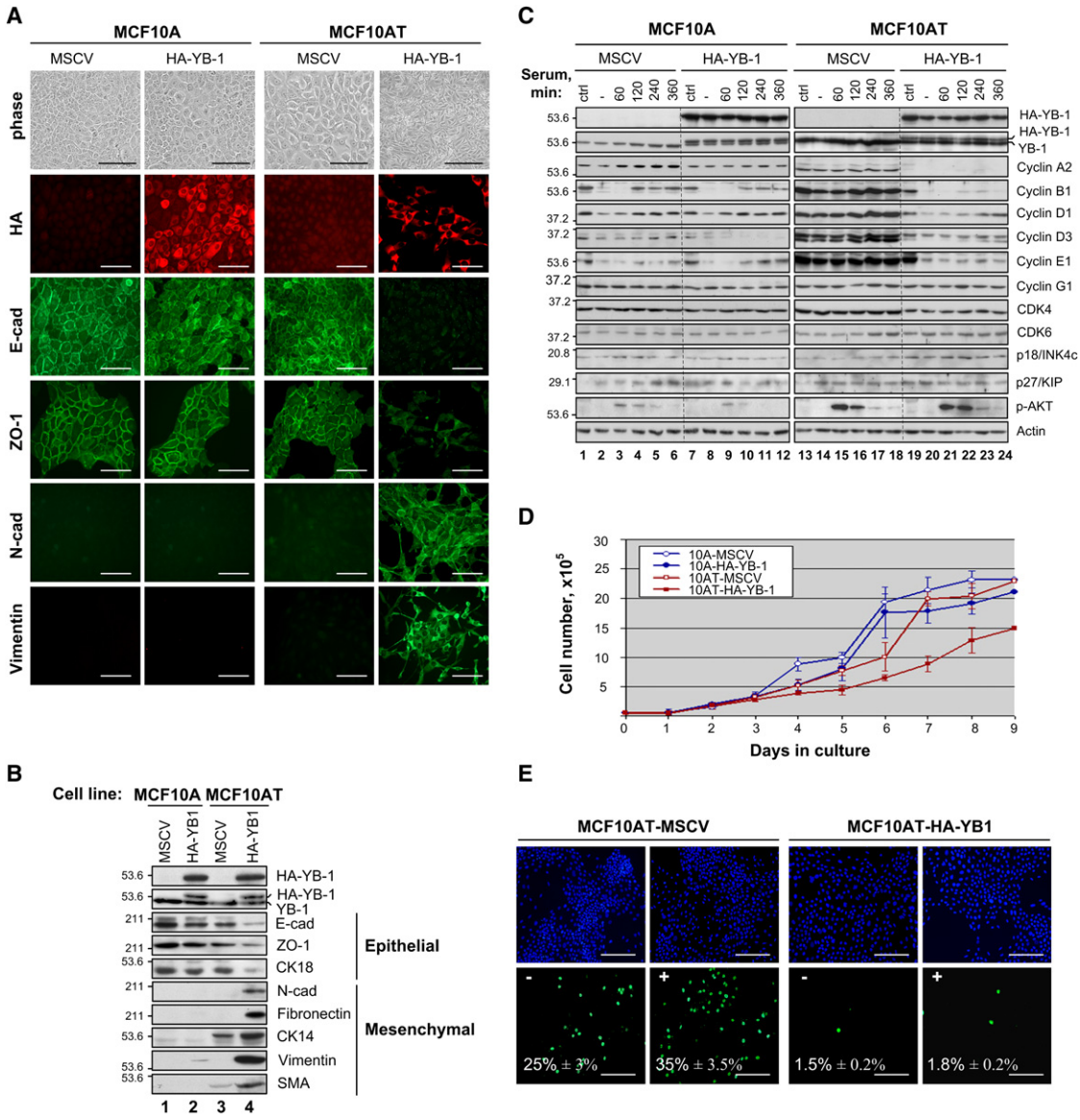

Figure 1. YB-1 Induces EMT and Reduces Proliferation of MCF10AT Cells

(A and B) MCF10A and MCF10AT cells expressing empty vector (MSCV) or HA-YB-1 were examined by phase contrast and immunofluorescence staining (A) or immunoblotting (B) for the expression of epithelial and mesenchymal markers. Scale bars, 100 μm.

(C) Expression patterns of cell-cycle-associated molecules in MCF10A and MCF10AT cell lines. Exponentially growing cells were either left untreated (ctrl) or serum starved for 24 hr (−) and then restimulated with complete medium for the times indicated. Response to serum was confirmed by Ser-473 phosphorylation of AKT.

(D) Growth curves of MCF10A and MCF10AT cell lines. Each data point represents the mean ± SD from three independent experiments in triplicate.

(E) Cell-cycle reentry of MCF10AT cells after serum starvation. Cells were serum starved for 24 hr and either left untreated (−) or restimulated with complete medium for 2 hr (+) and labeled with BrdU to visualize cells entering S phase. Percentage of BrdU-positive cells (green) was calculated relative to total cell populations (blue) in five random fields of view. Representative fields are shown. Scale bars, 100 μm. Averaged values from two independent experiments ± SD are indicated.

analyzing the effects of mutant YB-1 proteins on the phenotype of MCF10AT cells. Similar to wild-type YB-1, the YB-1 Ser102-to-Ala mutant protein, which cannot be phosphorylated by AKT and remains cytosolic (Bader and Vogt, 2007; Evdokimova et al., 2006b), still induced an EMT, while a truncated form of YB-1 (1–204), which localizes exclusively to the nucleus (Sorokin et al., 2005), did not (Figure S2B).

Given the mesenchymal phenotype of MCF10AT-YB-1 cells, we hypothesized that ectopic YB-1 expression may increase cell motility as a consequence of the EMT process. Indeed, time-lapse imaging during wound healing revealed that MCF10AT-YB-1 cells moved in a rapid and highly erratic fashion, in contrast to slower-moving MCF10AT-MSCV cells, which exhibited a more collective, directional migration pattern (Figures

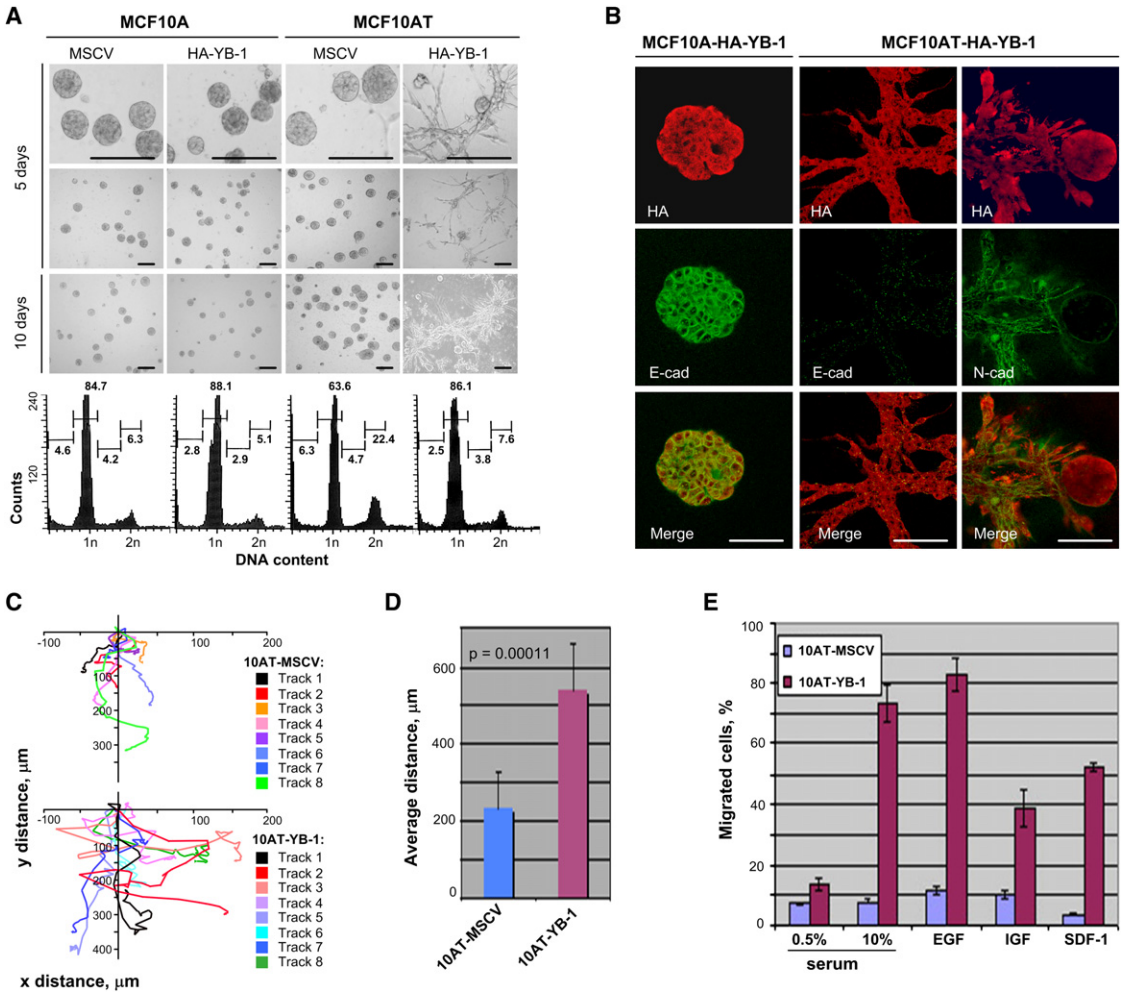

Figure 2. YB-1 Disrupts Mammary Acinar Architecture and Enhances Migration

(A) MCF10A and MCF10AT cell lines were grown on Matrigel for 5 or 10 days, as indicated. Three-dimensional structures were photographed by phase-contrast microscopy at low and high magnifications. Scale bars, 100 μm. Bottom panels depict cell-cycle distribution at day 5, as examined by FACS. Percentages of cells in sub-G1, G1, S, and G2/M are indicated. Data shown are representative of three independent experiments.

(B) Three-dimensional structures produced by MCF10A-YB-1 and MCF10AT-YB-1 cells were examined for E-cadherin or N-cadherin expression by confocal microscopy. Ectopic expression of HA-YB-1 and its cytosolic localization was confirmed by staining with anti-HA antibodies. Scale bars, 50 μm.

(C) Migration patterns of individual cells as determined by time-lapse imaging. The migration paths of eight cells taken from the wound edge for MCF10AT-MSCV (top panel) and MCF10AT-YB-1 (bottom panel) cells are plotted as an x and y axis migration profile.

(D) Comparison of the average distance traveled ± SD for eight cells tracked in (C).

(E) Migration of MCF10AT cell lines toward serum or growth factors as determined by transwell migration assays. Migration toward 0.5% serum was used as a negative control. The results of two independent experiments counted in triplicate are represented as a mean ± SD.

2C and 2D and data not shown). In addition, serum-starved MCF10AT-YB-1 cells displayed a remarkable capacity for migration in response to serum, epidermal growth factor, insulin-like growth factor-1, or stromal-derived factor 1 (Figure 2E), suggesting that they can migrate toward gradients of specific growth factors and chemokines generated in a tumor microenvironment. The difference in migration between vector alone and YB-1-overexpressing MCF10AT cells was highest when cells were serum starved prior to the assay (data not shown), raising the possibility that the migratory phenotype induced by YB-1 may provide starving cells with the ability to colonize nutrient-rich areas.

YB-1 and Ras-ERK Signaling Are Both Required for Induction of EMT

To examine if elevation of YB-1 is directly responsible for the observed EMT in MCF10AT cells, transient transfection with a pool of four different siRNA oligonucleotides was utilized to specifically reduce YB-1 expression in MCF10AT-YB-1 cells. Due to extensive protein stability, substantial reduction of YB-1 protein levels was observed only by day 4 after transfection, with a concomitant induction of cyclins B1, D1, and D3 (but not E1 and G1) (Figure 3A). This further confirms that YB-1 is directly responsible for blocking expression of these proteins, although the delayed kinetics of cyclin D3 induction may indicate additional

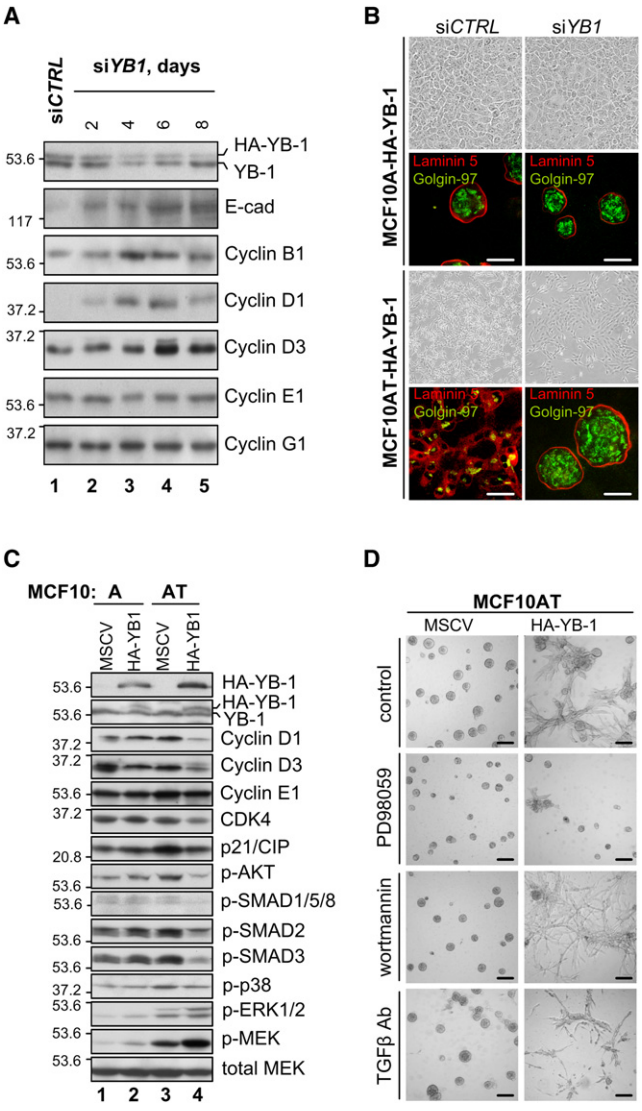

Figure 3. YB-1 and Ras-ERK Signaling Are Both Required for Induction of EMT

(A) MCF10AT-YB-1 cells transiently transfected with 20 nM of scrambled (si*CTRL*) or *YB-1* (si*YB-1*) siRNA pools were examined for the expression of YB-1 and potential YB-1 target proteins by immunoblotting. Cyclin G1 was used as a loading control.

(B) MCF10A and MCF10AT cell lines were transiently transfected with 20 nM si*CTRL* or si*YB-1* and either left on plastic or re-plated on Matrigel 24 hr after transfection. Morphology was examined 4 days after by phase-contrast (top panels) or confocal (bottom) microscopy. Scale bars, 25 μM.

(C) MCF10A and MCF10AT cell lines were grown on Matrigel for 5 days and then examined for the expression of cell cycle and signaling molecules by immunoblotting.

(D) MCF10AT cell lines growing on Matrigel in low-serum assay medium were treated with 50 μM PD98059, 0.1 μM wortmannin, or 20 μg/ml of pan-TGF-β-neutralizing antibodies for 10 days. Inhibitors were added the day after plating. Scale bars, 100 μm.

regulatory mechanisms at the level of transcription or mRNA stability. Reduced expression of YB-1 was also associated with reexpression of E-cadherin and downregulation of N-cadherin, vimentin, and SMA (Figure 3A and see Figures 7C and 7D), consistent with restoration of the epithelial phenotype. When placed in Matrigel, ~30% of *YB-1* siRNA-transfected MCF10AT-YB-1 cells regained the ability to form acinar structures, whereas cells transfected with control siRNA retained a fibroblastoid phenotype (Figure 3B, bottom panels). Considering that the transfection efficiency in the MCF10AT-YB-1 cell line was ~30%–50% (see Figure 7D, middle panel), we conclude that cells lacking YB-1 regained the ability to form acinar structures. Nevertheless, it seems likely that YB-1 itself is not required for normal acinar morphogenesis, as depletion of YB-1 in MCF10A cells had no effect on acinus formation (Figure 3B, top panels). The acini formed by si*YB-1*-treated MCF10AT-YB-1 cells exhibited proper apicobasal polarization, as shown by the apical orientation of the Golgi protein golgin-97 and basal deposition of the extracellular matrix protein laminin 5 (Figure 3B). However, consistent with the antiproliferative activity of YB-1, acinar structures formed by *YB-1* knockdown cells failed to form hollow lumens and did not undergo growth arrest. After day 8 they began to revert to a more disrupted acinar architecture (data not shown), which correlated with reexpression of YB-1 (Figure 3A, lane 5). Therefore, in vitro acinar morphogenesis and EMT induction are inversely dependent on the expression levels of YB-1.

Next we analyzed major signaling pathways that might contribute to the observed phenotypic changes in 3D cultures. Not surprisingly, Ras-ERK signaling was activated in MCF10AT cells, as evidenced by elevated levels of phosphorylated ERK1/2 (p-ERK) and MEK (p-MEK) (Figure 3C, lane 3). For unclear reasons, in MCF10AT-YB-1 cells, p-ERK1/2 and p-MEK levels were even higher than in MCF10AT-MSCV cells (Figure 3C, compare lanes 3 and 4). In contrast, PI3K-AKT and TGF-β pathway activities were reduced in MCF10AT-YB-1 cells based on decreased levels of p-AKT and p-SMAD proteins, respectively (Figure 3C). To more rigorously assess if these pathways might contribute to YB-1-associated EMT, we tested whether the MEK inhibitor PD98059, the PI3K inhibitor wortmannin, or pan-TGF-β-neutralizing antibodies could influence YB-1-mediated phenotypic changes. As shown in Figure 3D, inhibition of Ras-ERK signaling but not TGF-β or PI3K-AKT pathways completely abolished formation of cord-like structures in MCF10AT-YB-1 cells, while only slightly reducing growth of acinar structures in the other cell lines. Therefore, Ras-ERK but not PI3K-AKT or TGF-β signaling appears to be crucial for the observed YB-1-mediated phenotypic effects in MCF10AT cells. These data demonstrate the necessity of both hyperactivated Ras-ERK signaling and elevated YB-1 levels for the observed EMT in MCF10AT cells.

Ectopic Expression of YB-1 in MCF10AT Cells Confers Invasive and Metastatic Ability

To study the in vivo consequences of YB-1 overexpression in premalignant breast epithelial cells, MCF10AT-MSCV or MCF10AT-YB-1 cells were orthotopically injected into mouse mammary fat pads. By 3 months after injection, MCF10AT-MSCV cells were detected as multicellular E-cadherin- and cytokeratin-positive tumor lesions with glandular differentiation that were strictly localized to the fat pad injection sites (Figure 4A). In marked contrast, MCF10AT-YB-1 cells were diffusely disseminated throughout the fat pads as single cells or tiny clusters. Cells were negative for E-cadherin but positive for N-cadherin, myoepithelial markers p63 and SMA, and epithelial cytokeratins

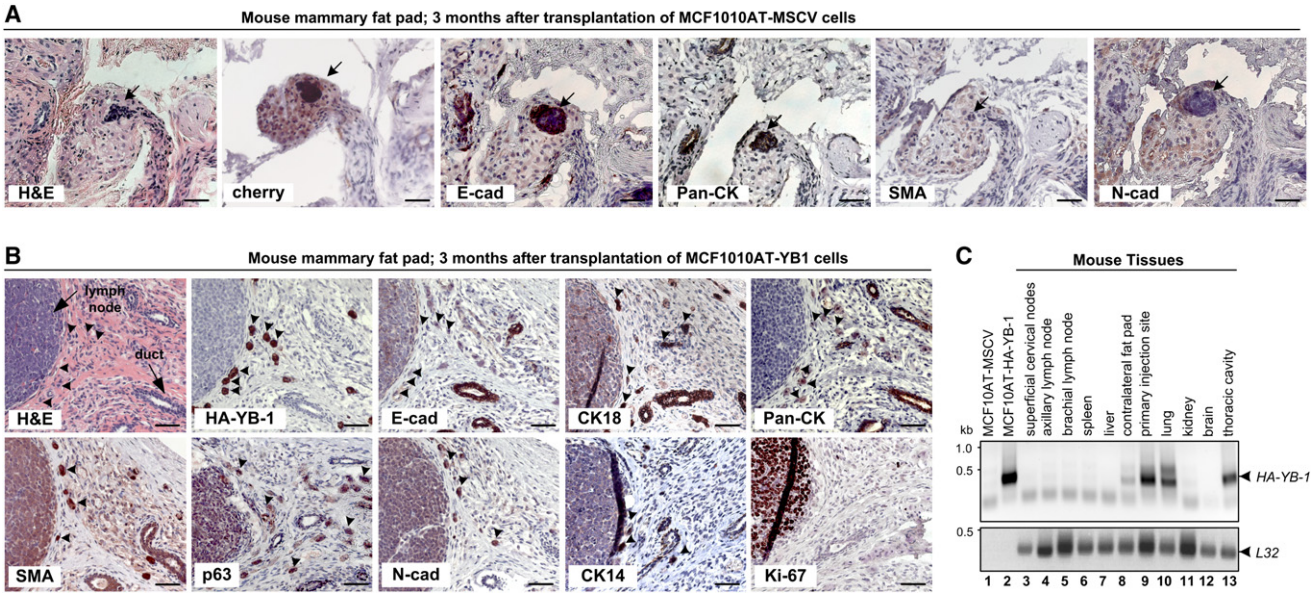

Figure 4. Ectopic Expression of YB-1 in MCF10AT Cells Confers Invasive and Metastatic Ability

(A and B) Hematoxylin and eosin (H&E) and immunohistochemical staining of mouse mammary fat pad sections 3 months after orthotopic transplantation of Cherry-expressing MCF10AT-MSCV (A) or MCF10AT-YB-1 (B) cells. Arrows in (A) depict hyperplastic mCherry-positive lesions, positive for E-cadherin and pan-CK and negative for SMA and N-cadherin. Arrowheads in (B) depict HA-YB-1-positive cells, negative for E-cadherin and Ki-67 and positive for pan-CK, CK18, CK14, N-cadherin, p63, and SMA. Scale bars, 50 μm.

(C) Expression of *HA-YB-1* mRNA was examined by semiquantitative RT-PCR in mouse tissues 3 months after orthotopic transplantation of MCF10AT-YB-1-mCherry cells. Total RNAs isolated from MCF10AT-MSCV and MCF10AT-YB-1 cells (lanes 1 and 2) were used as negative and positive controls, respectively. Endogenous mouse *L32* mRNA levels were used as an internal loading control.

(Figure 4B), consistent with these being epithelial cells having undergone an EMT. Among the 20 mice analyzed from two independent experiments, none of the MCF10AT-YB-1 mice developed the larger lesions localized to injection sites that were characteristic of MCF10AT-MSCV mice, suggesting that the observed dissemination of MCF10AT-YB-1 cells was not simply due to differential injection of the cells within the mammary fat pads. Their inability to grow in mouse fat pads may be explained by their low-proliferative potential in vitro (Figures 1D and 1E) and in vivo, based on Ki-67 staining of the fat pads (Figure 4B). Interestingly, MCF10AT-YB-1 cells exhibited mixed expression of luminal (CK18) and basal (CK14) cytokeratins, which is also consistent with their in vitro phenotype (Figure 1B). Moreover, these cells were also present in the thoracic cavities and lungs of MCF10AT-YB-1 mice, as confirmed by RT-PCR detection of *HA-YB-1* transcripts (Figure 4C). Therefore, despite the failure to develop microscopic tumor masses within the 3 month observation period, MCF10AT-YB-1 cells appear to have gained the ability to survive and infiltrate surrounding tissue and distant organs. These results provide strong evidence that increased expression of YB-1 in premalignant mammary epithelial cells with elevated Ras-ERK signaling not only blocks proliferation but disrupts mammary morphogenesis and promotes invasive properties and cell dissemination.

Mesenchymal-Like YB-1$^+$E-cadherin$^-$ Cells Exhibit Invasive Behavior in Human Breast Cancers

To evaluate the potential pathophysiological relevance of our findings, we used double immunofluorescence to compare patterns of YB-1 expression in normal breast epithelium and human breast carcinomas. Similar to nontransformed MCF10A cells, YB-1 was coexpressed with E-cadherin in normal mammary acini and localized exclusively to the cytosol of ductal luminal cells (Figure 5A). YB-1 was absent in the outer SMA- and p63-positive myoepithelial cell layer as well the subjacent stroma, indicating a highly restricted pattern of expression. Likewise, in ductal carcinoma in situ (DCIS), a known precursor of invasive breast cancer, neoplastic ducts were positive for both E-cadherin and YB-1 and the surrounding myoepithelial layer was negative for YB-1 (Figure 5B). Unexpectedly, in several DCIS cases we noted disseminated tumor cells in subjacent stroma that were positive for both YB-1 and SMA, but negative for E-cadherin (Figure 5B), suggesting that EMT may be an early event in DCIS progression. In invasive ductal carcinoma (IDC) cases, YB-1-positive cells lacking E-cadherin could readily be found in disseminated clusters of tumor cells penetrating into the surrounding stroma that were clearly separate from E-cadherin-positive cell clusters (Figure 5C). Although these IDC cases were classified as high-grade luminal tumors, scattered YB-1$^+$E-cadherin$^-$ cells were also positive for SMA and occasional cells costained for p63, thereby confirming their epithelial origin. Coexpression of YB-1 and p63 in these cells also clearly distinguishes them from normal myoepithelial cells that are negative for YB-1 (Figure 5A) and may be indicative of their progenitor-like properties. Similar to MCF10AT-YB-1 cells in mouse studies (Figure 4B), invasive YB-1-positive cells were low or nonproliferating, as demonstrated by their lack of staining for the proliferation markers Ki-67, PCNA, and cyclin D1 using morphometric

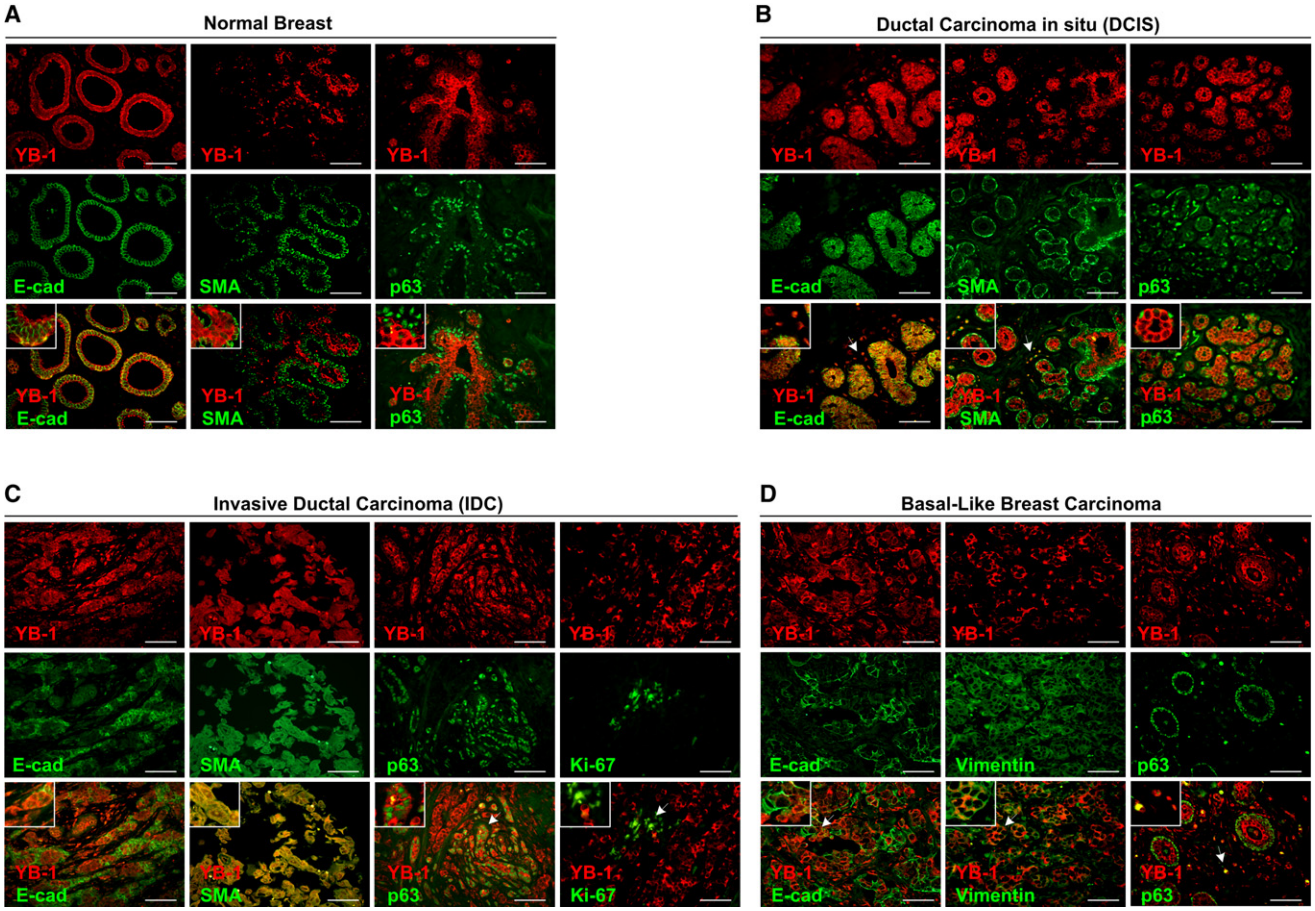

Figure 5. Mesenchymal-Like YB-1$^+$E-Cadherin$^-$ Cells Exhibit Invasive Behavior in Human Breast Cancers

(A–D) Normal human breast tissues, DCIS, and IDC cases were examined for expression of endogenous YB-1, E-cadherin, SMA, p63, Ki-67, and vimentin by immunofluorescence microscopy. Note that in normal and DCIS cases the expression of SMA and p63 was limited to myoepithelial layers negative for YB-1 and E-cadherin. Arrows depict disseminated tumor cells positive for YB-1, SMA, and p63 and negative for E-cadherin. Inset boxes show the corresponding areas under higher magnification. Scale bars, 100 μm.

analysis (Figure 5C and Figures S3A and S3B). We also analyzed three cases of basal-like carcinoma thought to represent a distinct subtype of IDC with properties common to breast myoepithelial or even progenitor cells (Korsching et al., 2008) and which are reported to express high YB-1 levels (Stratford et al., 2007). Similar to invasive areas in other forms of IDC, there was a reverse correlation between YB-1 and E-cadherin levels, and some areas of basal-like tumors were positive for YB-1 and vimentin (Figure 5D). However, only occasional cells were positive for both YB-1 and p63, and none for YB-1 and SMA (Figures 5D and data not shown), suggesting that coexpression of YB-1 with specific myoepithelial/mesenchymal markers varies depending on the breast cancer subtype. Together, these data indicate that as DCIS progresses to IDC, there are increasing proportions of low-proliferative YB-1$^+$E-cadherin$^-$ cells with invasive properties.

We next performed immunohistochemical staining for YB-1 and E-cadherin on tissue microarrays containing duplicate cores of 143 in situ and IDC cases. This showed a statistically significant inverse correlation between YB-1 and E-cadherin expression levels in 65% of breast cancer specimens with strong YB-1 staining (32% of total cases; $p = 0.033$; see Figure S3C). Cases with strong E-cadherin and weak YB-1 expression consisted predominantly of DCIS or well-differentiated IDC cases, while those lacking E-cadherin but strongly positive for YB-1 tended to be high grade poorly-differentiated IDC (for representative examples, see Figure S3D). We then directly compared breast cancer-related survival in the strong YB-1/weak E-cadherin subset to the weak YB-1/strong E-cadherin subset by Kaplan-Meier analyses. There was no significant association between YB-1 expression alone and survival and only a trend toward increased survival with high E-cadherin expression alone (data not shown). However, compared to the cases with weak YB-1/strong E-cadherin, strong YB-1/weak E-cadherin expression correlated with significantly decreased breast cancer survival ($p = 0.0143$; Figure S3E). These findings provide compelling evidence that high YB-1 expression is associated with loss of E-cadherin in invasive and, therefore, potentially metastatic breast cancer cells and is indicative of poor clinical outcome.

YB-1 Translationally Activates a Subset of mRNAs Encoding EMT-Inducing Proteins

To better understand the mechanism underlying the EMT induction by YB-1, we performed microarray gene expression profiling on MCF10AT cell lines. Since YB-1 is known to exert its regulatory effects at the transcriptional as well as translational levels, we compared expression profiles of both total mRNAs and mRNAs isolated from polysomal (Ps; translationally active) or post-Ps (translationally inactive) fractions (Figure S4A). Compared to MCF10AT-MSCV cells, 296 mRNAs were concordantly downregulated in both total and Ps fractions from MCF10AT-YB-1 cells, while 88 transcripts were upregulated (Figure S5A). Consistent with the observed EMT in MCF10AT-YB-1 cells, expression of an epithelial mRNA cluster (E-cadherin, claudins 1, 4, and 7, desmoplakin, desmocollins 2 and 3, keratins 4, 15, 16, and 17, and integrins α6 and β6) was reduced in these cells, while multiple mesenchymal-associated mRNAs (N-cadherin, decorin, vimentin, fibronectin, and integrin α5) were significantly upregulated (Figures S5A and S5B and Table S1). Consistent with their dedifferentiated phenotype, MCF10AT-YB-1 cells also showed reduction of cell surface markers *CD24* and *CD82/KAI1* and elevation of *CD10*, *CD44*, and *CD68*.

Considering the predominantly cytosolic localization of YB-1 in our cell models, we hypothesized that some of the observed transcriptional changes might be secondary to changes in YB-1-mediated translational regulation of specific mRNA subsets. To identify such mRNAs, we analyzed transcripts that were equally expressed within total RNA populations of the two cell lines, but were selectively decreased or increased in Ps fractions from MCF10AT-YB-1 cells. Consistent with a cap-dependent translational repressor function for YB-1, the majority of transcripts (>80%) detected in Ps RNA preparations from MCF10AT-YB-1 cells were reduced relative to MCF10AT-MSCV cells. Among these were multiple cyclin mRNAs such as cyclin B1, D1, and D3 (Figures S4B and S4C), further supporting the direct involvement of YB-1 in their translational repression.

Surprisingly, however, we also identified a small subset of transcripts that were selectively enriched in Ps fractions from MCF10AT-YB-1 cells (Figure 6A). These included *Snail1* and other transcripts encoding well-known transcriptional inducers of EMT, such as two members of the high-mobility group transcription factor family, *Lef-1* and *TCF4*, the zinc finger/homeodomain transcriptional repressor *Zeb2/Sip1*, and hypoxia-inducible factor 1 α (*HIF1*α). The basic helix-loop-helix transcriptional regulator and EMT-inducer Twist was upregulated at both transcriptional and translational levels (Figure 6 and Table S1). There was also significant representation of messages implicated in early development and morphogenesis, as well as numerous transcription factors with unknown functions. These included two other Snail superfamily members, *Snail3* and *Scratch1*, and multiple members of zinc finger, basic helix-loop-helix, homeobox (HOX), and high-mobility group transcription factor families. Semiquantitative RT-PCR analysis using the corresponding primers (Table S4) showed that, with a few exceptions, the majority of these messages were indeed equally expressed in total RNA populations from both MCF10AT-MSCV and MCF10AT-YB-1 cell lines but selectively enriched in Ps RNA fractions from MCF10AT-YB-1 cells (Figure 6B). A corresponding increase in protein expression was confirmed by immunoblotting (Figure 6C). In addition to Snail1 and Twist, we observed elevated expression of Lef-1, Foxo3a, HoxC6, and HIF1α. Interestingly, some of these proteins, including Foxo3a and HoxC6, were translationally induced by YB-1 even in MCF10A-YB-1 cells, indicating that YB-1 may also translationally activate certain messages in nontransformed cells. In summary, we observed concordant translational activation of multiple EMT-associated factors in YB-1-overexpressing breast epithelial cells and their combined action is likely responsible for the switch from an epithelial to mesenchymal gene expression program.

Elevated Levels of YB-1 Correlate with Translational Induction of *Snail1* and Snail1-Mediated Loss of E-Cadherin in Multiple Cell Types

We next wished to confirm that YB-1 is required for translational activation of the major inducers of EMT identified in our study. We predominantly focused on Snail1 and Twist since their roles in EMT and breast cancer invasiveness are well established (Thiery and Sleeman, 2006). *Snai1l* transcripts were present in MCF10AT cell lines and not in their normal MCF10A counterparts and were translationally active predominantly in MCF10AT-YB-1 cells (i.e., present in Ps fractions and expressed at the protein level; see Figures 6B and 6C and Figure S6A). Expression of Twist was elevated in MCF10AT-YB-1 cells at both transcriptional and translational levels (Figures 6B and 6C). This is in contrast to the Snail1 homolog Snail2/Slug, whose expression levels were not changed in any of the cell lines analyzed (Figures 6B and 6C). Similar results were obtained using the nontransformed mouse mammary epithelial cell line EpH4 and its H-Ras-transformed counterpart. In contrast to parental EpH4 cells, ectopic expression of YB-1 in EpH4-H-Ras cells led to induction of Snail1, vimentin, and SMA, loss of E-cadherin expression, and disruption of mammary acinar architecture and polarity (Figures S1B and S1C). These results indicate that YB-1 induces Snail1 protein expression and EMT-like changes in Ras-transformed mammary epithelial cells of different origins and are consistent with previous findings showing that oncogenic H-Ras (G12V) activates the *Snail1* promoter in a Ras-ERK-dependent manner (Peinado et al., 2003). Similarly, *HoxC6* and *Zeb2* expression levels were reduced in MCF10AT-YB-1 cells by treatment with the MEK inhibitors UO126 or PD98059 but not with wortmannin (Figure S6B). Interestingly, *Twist* expression may require both Ras-ERK and PI3K-AKT signaling as it was inhibited by wortmannin to an extent comparable to that observed with MEK inhibitors. Therefore, it is likely that two sequential steps are required for expression of Snail1 and certain other EMT-inducing proteins: (1) transcriptional activation of the gene by elevated Ras-ERK signaling and (2) YB-1-dependent translational activation of the corresponding mRNA.

To further establish a link between YB-1, Snail1, and Twist expression levels, we analyzed a panel of metastatic versus nonmetastatic human cancer cell lines. Similar to invasive breast carcinoma cells (Figure 5C), endogenous levels of YB-1 were elevated exclusively in metastatic cell lines and correlated with the loss of E-cadherin and induction of Snail1, Twist, N-cadherin, and vimentin (Figure 7A). Notably, knockdown of *YB-1* in two mesenchymal-like cell lines, MDA-MB-231 and MDA-MB-435S, inhibited expression of Snail1 and Twist as well as

A

Gene name	Transcription factors with known function in EMT	Ps/Total ratio
HIF1α	Hypoxia-inducible factor 1, alpha; bHLH TF; angiogenesis; invasion; dedifferentiation	3.4
LEF-1	Lymphoid enhancer-binding factor 1, HMG box TF; cell differentiation, morphogenesis	2.1
SNAIL1	Snail homolog 1 (Drosophila); zinc finger TF; E-cad repressor; development; metastasis	2.0
ZEB2/SIP1	Zinc finger HOX 1b; SMAD interacting protein 1; TF; metastasis; development	1.6
TWIST	Twist homolog 1 (Drosophila); bHLH TF; induces *N-cad* & *fibronectin*; development; metastasis	1.4
SNAIL2/SLUG	Snail homolog 2 (Drosophila); zinc finger TF; development; metastasis	1.1
	Putative EMT inducers identified in MCF10AT-YB1 cells	
PRICKLE1	Prickle-like 1 (Drosophila); ZF, zinc-binding domain (LIM); putative repressor of Wnt/β-catenin	8.0
MORTALIN-2	Heat shock 70kDa protein 9B, pro-survival	7.9
MNT	MAX binding protein; bHLH-zipper domain; TF; repressor; c-myc antagonist; growth inhibitor	6.2
ELISC-1	ELISC-1; putative regulator of tumour invasiveness	5.8
PDEF	SAM pointed domain containing ETS TF; PSA transactivator; epithelium hyperplasia	5.0
ZHX1	Zinc fingers and homeoboxes 1; C2H2-type zinc fingers; putative transcriptional repressor	5.0
HOP	Homeodomain-only protein; TF; development; morphogenesis; tumor suppressor	4.5
SMO	Smoothened homolog; transmembrane receptor; hedgehog signal transducer; differantiation	4.0
SAP2/Net	ELK3, ETS-domain protein; growth supressor; inhibitor of G1-S; required for cell migration	3.7
ZNF37b	Zinc finger protein 37b (KOX 21); predicted protein; function is unknown	3.5
HAKAI	Cas-Br-M (murine); E3 ligase; E-cad degradation	3.3
YPEL2	Yippee-like 2 (Drosophila); ZF protein; potential function in cell division	3.1
ZFR	Zinc finger RNA binding protein; putative TF	3.1
ZNF621	Zinc finger protein 621; krueppel C2H2-type zinc-finger family; putative TF; repressor	3.1
ATAXIN 1	Ataxin 1; transcriptional regulator; development; neurogenerative disorders	3.0
LMO2	LIM domain only 2 (rhombotin-like 1); TF; putative E-cad repressor; hematopoiesis; leukemia	2.9
ZNF208	Zinc finger protein 208; krueppel C2H2-type zinc-finger protein family; putative TF	2.9
TCF4	ITF2/SEF2; bHLH; E-box binding; target of Wnt/TCF; development; neuronal plasticity	2.9
ZNF207	Zinc finger protein 207; C2H2 zinc finger; function is unknown	2.7
SESN3	Sestrin 3; antioxidant modulator; neuronal differentiation; polarity	2.6
HMG20B	High-mobility group 20B; putative transcriptional regulator; chromatin remodeling	2.5
LIMD1	LIM domains containing 1; putative growth suppressor; inhibitor of G1-S	2.5
ZNF417	Zinc finger protein 417; krueppel C2H2-type zinc-finger family; function is unknown	2.5
FOXO3a	Forkhead box O3A; endothelial cell morphogenesis and vascular homeostasis; oxidative stress	2.4
PBX1	Pre-B-cell leukemia TF 1; HOX 1; putative role in cell survival & neuronal differentiation	2.4
ZNF200	Zinc finger protein 200; C2H2 zinc finger; function is unknown	2.4
ZSWIM3	Zinc finger, SWIM domain containing 3; SWIM zinc finger; function is unknown	2.4
PES1	Pescadillo homolog 1, BRCT domain; cell cycle & Rs biogenesis; embryonic development	2.3
ATOH/MATH1	Atonal homolog 1 (Drosophila); bHLH; cell proliferation & differentiation; neurogenesis	2.3
HOXC6	Homeobox C6; TF; morphogenesis; differentiation; neuronal plasticity; anti-apoptotic	2.3
HOXC14	Homeobox C14; TF; function is unknown	2.2
ZNF286	Zinc finger protein 286; function is unknown	2.2
ZF-DHHC19	Zinc finger, DHHC domain (NEW1) containing 19; function is unknown	2.2
ZC3H6	Zinc finger CCCH type domain containing 6; function is unknown	2.1
ZNF212	Zinc finger protein 212; krueppel C2H2-type zinc-finger family; function is unknown	2.1
TOB2	Transducer of ERBB2, 2; transcriptional repressor; inhibitor of G1-S phase and growth	2.0
TGIF	TGFB-induced factor; TALE family homeobox; TF; co-repressor; neural development	2.0
ZNF224	BMZF2; krueppel C2H2-type zinc-finger family; putative TF; repressor; development	2.0
ZNF527	Zinc finger protein 527; krueppel C2H2-type zinc-finger family; function is unknown	2.0
SNAIL3	Snail homolog 3 (Drosophila); ZF TF; predicted protein; function is unknown	1.8
SCRATCH	Scratch homolog 1 (Drosophila); ZF TF, Snail family; putative role in neural differentiation	1.8

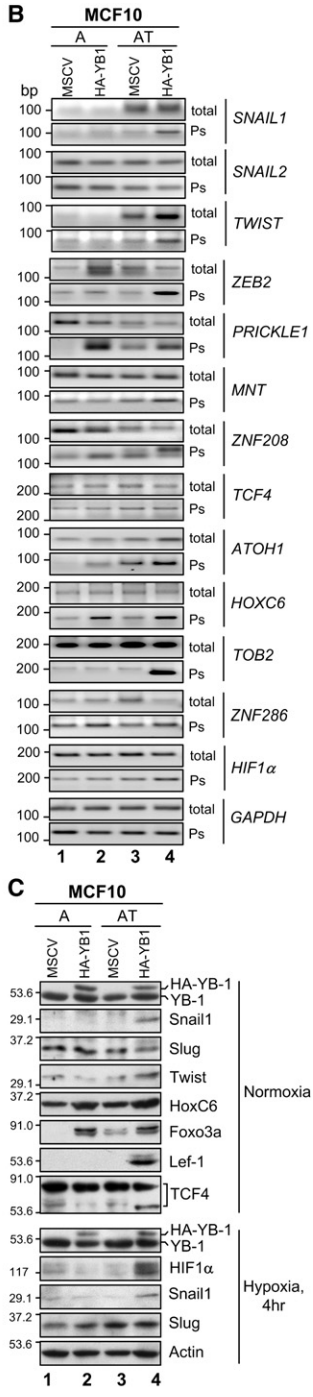

Figure 6. YB-1 Translationally Activates a Subset of mRNAs Encoding EMT-Inducing Proteins

(A) Candidate mRNAs identified by microarray analysis as being translationally activated (enriched in Ps fractions) in MCF10AT-YB-1 cells relative to MCF10AT-MSCV cells. Fold upregulation is measured as Ps/total RNA ratio.

(B) Levels of selected candidate mRNAs in total and Ps fractions from MCF10A and MCF10AT cell lines were examined by semiquantitative RT-PCR. Endogenous *GAPDH* mRNA level was used as an internal control.

(C) Protein expression of selected candidate proteins was confirmed by immunoblotting. Actin was used as a loading control.

N-cadherin, as shown by using several independent *YB-1* siRNAs (Figure 7B and Figure S6C). While MDA-MB-231 is well established as a metastatic breast cancer cell line, MDA-MB-435 cells are now known to derive from a metastatic melanoma (Rae et al., 2007), demonstrating potentially wider roles for YB-1 in epithelial malignancies. In agreement with a direct involvement of YB-1 in regulating cyclin D1 expression, YB-1 knockdown led to increased cyclin D1 levels (Figure 7B). Of further note,

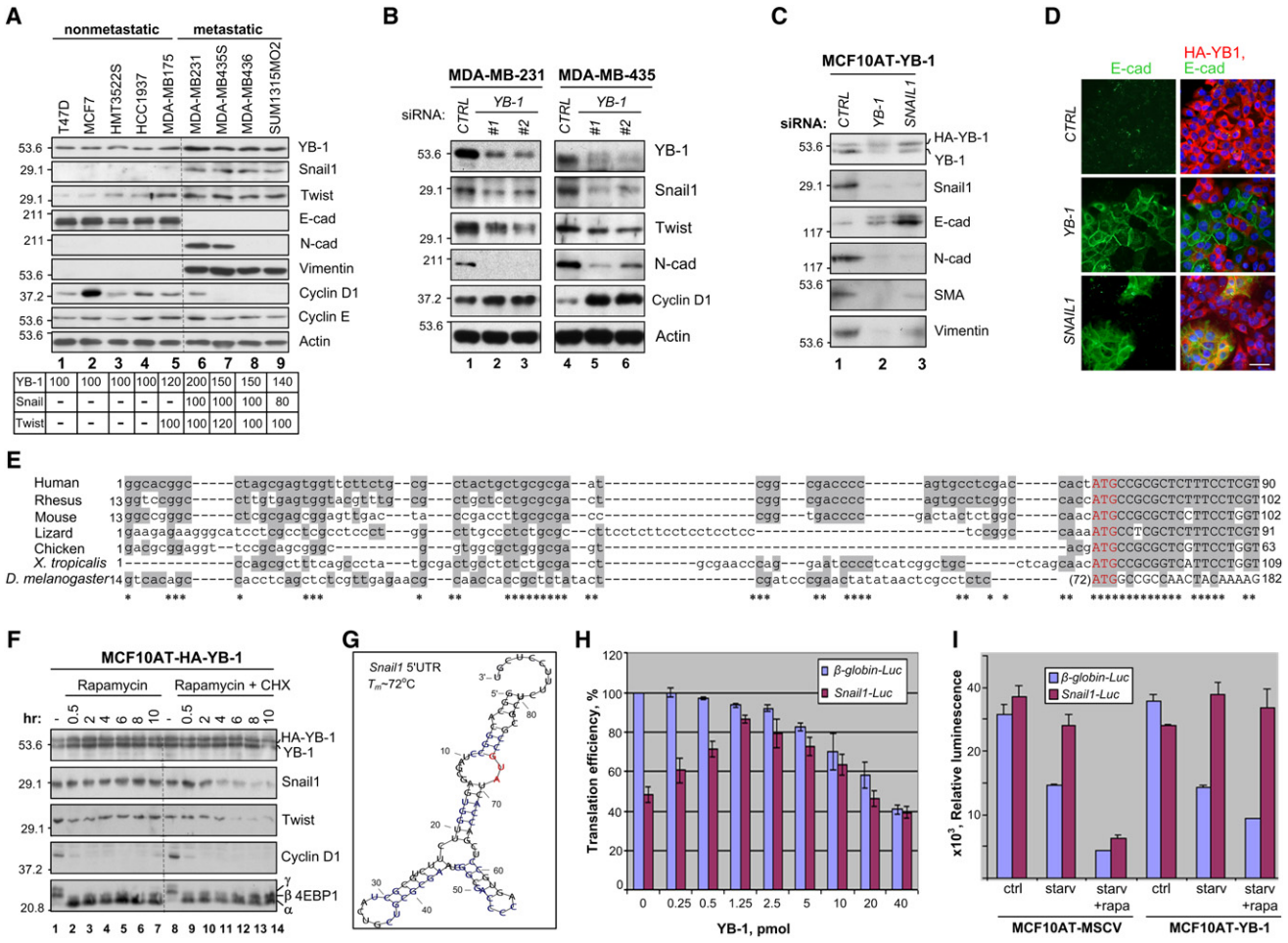

Figure 7. Efficient Translation of *Snail1* mRNA Requires Elevated Levels of YB-1

(A) Expression of YB-1, Snail, Twist, and their downstream targets in immortalized nontransformed mammary epithelial cells (HMT3522S), nonmetastatic breast cancer cell lines (T47D, MCF7, HCC1937, and MDA-MB175), and metastatic breast cancer (MDA-MB-231, MDA-MB-436, and SUM1315MO2) and melanoma (MDA-MB-435S) cell lines was examined by immunoblotting. Relative amounts of YB-1, Snail1, and Twist averaged from three independent experiments are indicated at the bottom.

(B) MDA-MB-231 or MDA-MB-435S cells were transiently transfected with 25 nM of scrambled (*CTRL*) or *YB-1* siRNAs. The expression of YB-1, Snail1, Twist, and their downstream targets was examined by immunoblotting 4 days after transfection.

(C and D) MCF10AT-YB-1 cells were transiently transfected with 20 nM of scrambled (*CTRL*), *YB-1*, or *SNAIL1* Smart siRNA pools. The expression levels of YB-1, Snail1, and their downstream targets were examined 4 days later by immunoblotting (C) or immunofluorescence microscopy (D). Scale bars, 25 μm. Note that some cell clusters remained positive for YB-1 and negative for E-cadherin, likely reflecting 30%–50% transfection efficiencies.

(E) Alignment of *Snail1* 5′UTRs from different species. Asterisks indicate conserved nucleotides.

(F) Immunoblot of Snail1, Twist, and cyclin D1 expression in MCF10AT-YB-1 cells treated with 50 nM rapamycin ± cycloheximide (CHX; 20 μg/ml). 4E-BP1 phosphorylation pattern confirms blockade of the mTOR pathway by rapamycin.

(G) Analysis of the human *Snail1* 5′UTR secondary structure using Vienna RNA secondary structure prediction tool (http://rna.tbi.univie.ac.at/cgi-bin/RNAfold.cgi). The start AUG codon is shown in red and the conserved nucleotides are marked blue.

(H) Capped *Luc* mRNA (40 ng; ~0.067 pmol) harboring 5′UTRs of either *β-globin* or *Snail1* were incubated in rabbit reticulocyte lysates in the absence or presence of increasing amounts of YB-1. After 60 min incubation at 30°C, translation reactions were resolved by 10% SDS-PAGE and [^{35}S]methionine-labeled translation products were detected by autoradiography. Results of four independent experiments were quantified by phosphorimaging software and the data are presented as mean ± SD.

(I) pcDNA3 plasmids encoding firefly Luc under control of the 5′UTR of either *β-globin* or *Snail1* were transiently transfected into MCF10AT-MSCV or MCF10AT-YB-1 cells, along with a renilla Luc reporter (pRL) for normalization. Where indicated, cells were starved prior to transfection or starved and simultaneously treated with 50 nM of rapamycin (see Supplemental Experimental Procedures). Luciferase activities were measured after 24 hr. The data are mean ± SD of three separate transfections performed in duplicate.

inhibition of Snail1, Twist, and N-cadherin paralleled downregulation of YB-1 and was detected as early as day 4 after transfection, whereas reexpression of the epithelial markers E-cadherin and ZO-1 was significantly delayed (Figure S6C), suggesting that additional factors may be necessary for complete reversion of the mesenchymal phenotype.

We next wished to test whether YB-1 is directly responsible for the enhanced expression of Snail1 and loss of E-cadherin and

that it acts upstream of Snail1. Indeed, knockdown of *YB-1* in MCF10AT-YB-1 cells resulted in virtually undetectable Snail1 protein levels, whereas *Snail1* knockdown did not affect YB-1 expression (Figure 7C). As expected, MCF10AT-YB-1 cells with reduced Snail1 levels regained expression of E-cadherin and lost that of N-cadherin, vimentin, and SMA (Figures 7C and 7D). However, in contrast to *YB-1* knockdown cells in which there was clear membrane localization of E-cadherin, in cells treated with *Snail1* siRNAs E-cadherin localization was diffuse, with a significant portion remaining cytosolic (Figure 7D). Also, in contrast to *YB-1* knockdown (Figure 3B), MCF10AT-YB-1 cells with *Snail1* knockdown failed to re-form acinar structures when grown in Matrigel (data not shown). Therefore, although Snail1 appears to be at least partially responsible for disrupted polarity and loss of E-cadherin in MCF10AT-YB-1 cells, additional EMT-inducing factors must be inactivated in these cells to fully restore their epithelial phenotype. Candidates include Twist and other factors identified in our studies and experiments are underway to investigate these possibilities.

YB-1 Stimulates Translation of *Snail1* mRNA While Inhibiting Cap-Dependent Translation

We next investigated the mechanism of translational activation of *Snail1* mRNA in MCF10AT-YB-1 cells. The fact that *Snail1* is translationally activated in the presence of the known cap-dependent translational repressor YB-1 points to the possibility of cap-independent translation initiation. This was further supported by the results showing that rapamycin, which is known to inhibit cap-dependent but not cap-independent translation (Beretta et al., 1996), did not affect Snail1 levels in MCF10AT-YB-1 cells, while completely abolishing cyclin D1 expression (Figure 7F, lanes 1–7). Maintenance of Snail1 expression in the presence of rapamycin was not due to increased Snail1 protein stability, as cotreatment of MCF10AT-YB-1 cells with the protein synthesis inhibitor cycloheximide resulted in rapid disappearance of Snail1 (Figure 7F, lanes 8–14). Thus, Snail1 expression under these conditions is due to continuing eIF4E- and cap-independent translation initiation. Similar patterns of Twist expression (Figure 7F) suggest a cap-independent translation initiation mechanism as well.

To determine whether *Snail1* mRNA harbors specific regulatory motifs in its 5′UTR that are responsible for its cap-independent translation initiation, the human *Snail1* mRNA 5′UTR was compared to other species. With the notable exception of *Drosophila*, *Snail1* mRNA 5′UTRs from primates, mouse, lizard, chicken, and *Xenopus* are relatively short (~70 nucleotides) and contain several highly conserved G-C-enriched nucleotide clusters (Figure 7E). *Snail1* 5′UTRs from these different species are predicted to form similar highly stable stem-loop structures with conserved nucleotides mapping primarily to the stem regions, whereas the 4- to10-nt-long loops exhibit a high degree of variability (Figure 7G). Such evolutionary conservation and complex secondary structure may be indicative of an internal ribosome entry site (IRES), which is known to mediate cap-independent translation initiation (Stoneley and Willis, 2004). This possibility was further supported by in vitro translation experiments. Using a reporter *Luc* mRNA linked to the 5′UTR of either *Snail1* or control *β-globin* for in vitro translation experiments, we found that in contrast to 5′*β-globin-Luc*, translation efficiency of 5′*Snail1-Luc* mRNA was independent of the presence or absence of a cap structure (data not shown) and was substantially lower than that of 5′*β-globin-Luc* mRNA (Figure 7H). Furthermore, YB-1 inhibited cap-dependent translation of 5′*β-globin-Luc*, while stimulating translation of 5′*Snail1-Luc* mRNA (Figure 7H). Further elevation of YB-1 above the physiological threshold resulted in translational repression of both mRNAs studied, consistent with the reported nonspecific translation inhibitory activity of YB-1 (Evdokimova et al., 2001). Transient transfection experiments revealed that despite similar translational activities of both 5′*β-globin-Luc* and 5′*Snail1-Luc* constructs in exponentially growing vector alone or YB-1-overexpressing MCF10AT cell lines, translation of 5′*Snail1-Luc* in MCF10AT-YB-1 cells was substantially higher under conditions of starvation or starvation combined with rapamycin treatment (Figure 7I). These results suggest that the 5′UTR of *Snail1* mRNA potentially contains an IRES element that mediates cap-independent translation initiation, especially under conditions where cap-dependent translation is restricted by nutrient deprivation. Given YB-1's ability to inhibit cap-dependent translation and to stimulate IRES-driven translation initiation (Cobbold et al., 2007; Evdokimova et al., 2006b), we thus propose that YB-1 positively regulates *Snail1* mRNA translation via an IRES-dependent translation initiation mechanism.

DISCUSSION

This study presents a distinctive model of gene regulation during metastatic progression, in which translational regulation by YB-1 is a restriction point controlling the coordinated repression of genes associated with cellular proliferation and the epithelial phenotype, while facilitating activation of a mesenchymal gene expression program. Induction of the latter appears to be a two-step mechanism involving Ras-ERK-dependent transcription of *Snail1* and other developmentally regulated genes and YB-1-mediated translation of the corresponding messages into protein products. In turn, these newly expressed pleiotropically acting proteins are responsible for subsequent transcriptional repression of E-cadherin and other epithelial genes and activation of mesenchymal genes (for a model, see Figure S7). Consistent with its important role in triggering a mesenchymal-like phenotype, YB-1 expression in human breast cancers and in MCF10AT cells injected into mouse mammary fat is associated with microinvasion and metastatic dissemination of low-proliferating mesenchymal-like cells.

Expression of YB-1 in normal breast epithelium and its cytosolic localization suggest an important role for YB-1 in restricting cap-dependent translation of growth-related mRNAs. YB-1 upregulation observed in multiple human malignancies may thus represent an adaptive cellular mechanism directed to overcome uncontrolled proliferation. On the other hand, YB-1 was reported to induce IRES-dependent translation of certain mRNAs (Cobbold et al., 2007) and, in our study, was indispensable for translational activation of a subset of mRNAs whose protein products are involved in morphogenesis and tumor progression. Among them, we identified Snail1, Twist, Zeb2/Sip1, HoxC6, Foxo3a, HIF1α, Lef-1, and others. Transcription of many of the corresponding mRNAs occurs during normal early embryonic development and is likely activated in carcinoma cells

due to abnormally high Ras-ERK signaling. Consistent with this, inhibition of Ras-ERK but not PI3K-AKT signaling in our experimental system reduced the expression levels of *Snail1*, *Twist*, *HoxC6*, and *Zeb2* mRNAs. Translation of at least some of these mRNAs, including *HIF1α* and *Lef-1*, was previously reported to be driven by IRES elements that allow for their selective translation during hypoxia and starvation (Jimenez et al., 2005; Lang et al., 2002; Stoneley et al., 2001). Our data indicates that the *Snail1* 5′UTR allows translation of a reporter mRNA under conditions of starvation and inhibition of cap-dependent translation in a YB-1-dependent manner (Figures 7F and 7I). Therefore, an intriguing possibility is that YB-1 contributes to inhibition of cap-dependent translation of growth-related mRNAs while simultaneously activating IRES-dependent translation of the aforementioned messages in hypoxic and nutrient-deprived tumor areas, thereby promoting acquisition of a mesenchymal-like migratory properties and facilitating tumor spread.

Although the link between YB-1 upregulation and tumor aggressiveness is well established (Bergmann et al., 2005; Janz et al., 2002), the precise mechanism has remained largely unknown. Our findings suggest that YB-1 operates upstream of key cellular pathways contributing to metastatic competence and tumor dormancy. For instance, by enabling expression of multiple embryonic transcription factors in carcinoma cells, YB-1 activates an EMT program that is normally functional in early embryogenesis. An important finding of this study is that it is not a single factor but likely a complex network of transcriptional regulators that is translationally controlled by YB-1. In addition to well-established EMT inducers such as Snail1, Twist, and Zeb2, which are known to mediate metastatic tumor progression and tumor recurrence in breast cancer (Barrallo-Gimeno and Nieto, 2005; Moody et al., 2005; Peinado et al., 2007; Yang et al., 2006), we identified several other potential EMT regulators whose activities may have equal importance in these processes. Among these are homeodomain-containing protein HoxC6 and c-Myc antagonist/growth inhibitor Mnt, which are both involved in mammary morphogenesis (Garcia-Gasca and Spyropoulos, 2000; Toyo-oka et al., 2006), and a regulator of cell movement and polarity, PRICKLE1 (Katoh, 2005). Although the role of these proteins in EMT remains to be proven, the majority function as transcriptional repressors and inhibitors of cell growth. Given the coordinated switch in gene expression profiles observed when MCF10AT cells overexpress YB-1, it is likely that these YB-1-induced transcription factors act in concert to inhibit growth-related and epithelial genes and to activate mesenchymal genes, potentially leading to invasive and metastatic behavior.

Upregulation by YB-1 of a large number of growth suppressors, including Snail1 and Zeb2 themselves (Mejlvang et al., 2007; Vega et al., 2004), is striking since tumorigenesis is typically associated with increased cell proliferation. It is tempting to speculate that antiproliferative activity is a common feature of EMT-promoting proteins and an integral part of the mesenchymal phenotype, allowing migrating embryonic or cancer cells to reach their destinations before resuming growth. Subsequent inactivation of this growth-suppressive program could be a very inefficient process, as solitary disseminated tumor cells may be detected in bone marrow and distant organs years before the development of overt metastasis, remaining viable yet unable to reenter the cell cycle (Brackstone et al., 2007; Gupta and Massagué, 2006). These slow-growing, nonapoptotic but highly mobile tumor cells are likely to be insensitive to therapeutic interventions that primarily target proliferating cells. Their inability to proliferate may also explain why mesenchymal-like cells are rarely detected in human carcinomas. Interestingly, MCF10AT-YB-1 cells appear to possess several stem cell properties, including low proliferation rates, upregulation of the stem cell markers p63, *CD44*, and *CD10*, and downregulation of *CD24*. Further studies are necessary to determine whether YB-1 expression and upregulation of EMT inducers is correlated with a stem cell phenotype, particularly in light of recent data suggesting a link between stem cells and EMT in breast cancer (Mani et al., 2008).

EXPERIMENTAL PROCEDURES

Cell Cultures and Xenografts

MCF10A and MCF10AT (MCF10AT1k.cl2) cell lines were obtained from Dr. Fred Miller and cultured as previously described (Debnath et al., 2003). SUM1315MO2 was obtained from Asterand. The other breast cancer cell lines, HeLa, and PC3 cells were purchased from American Type Culture Collection. The biological characteristics and culture conditions for each cell line are summarized in Table S2. Stable polyclonal cell lines expressing vector alone or HA-tagged YB-1 were generated by retroviral infection as described previously (Sorokin et al., 2005). For in vivo bioluminescent studies, cells were engineered to express mCherry, selected by FACS sorting, tested for expression of characteristic markers, and orthotopically transplanted (5×10^5 in 50 μl PBS) into the mammary glands of NOD/SCID mice. Three months after surgery different tissues were formalin fixed (for immunohistochemistry) or flash frozen (for RNA isolation and immunoblotting). Animal experiments were conducted following protocols approved by the University of British Columbia's Animal Care Committee.

Clinical Samples

A tissue microarray consisting of 175 cases of in situ and invasive breast cancer in duplicate was constructed from formalin-fixed paraffin-embedded tissues sent to the Vancouver General Hospital. Clinical follow-up data for 20 years was available for each case. This study was approved by the Clinical Research Ethics Board of the University of British Columbia (HO6-70105), and all patient identifiers were removed from the samples prior to analysis.

Cell Fractionation, RNA Isolation, and Microarray Analysis

Total cell extracts were prepared from subconfluent cells using Nonidet P-40 lysis buffer (20 mM HEPES-KOH [pH 7.6], 100 mM KCl, 5 mM $MgCl_2$, 2 mM dithiothreitol, 0.25% Nonidet P-40, 2 μg/ml leupeptin, 2 μg/ml pepstatin, and 10 μg/ml cycloheximide). Cell fractionation and purification of Ps and post-Ps fractions were performed as previously described (Evdokimova et al., 2006b; Sorokin et al., 2005). Five micrograms of each RNA sample was used for microarray probe synthesis and hybridization as described in the Affymetrix GeneChip manual. For each fraction, two independently isolated RNA samples were hybridized to Affymetrix GeneChip Human Exon 1.0 ST (HuEx 1.0) arrays. Gene-level signal estimates were derived from the CEL files by RMA-sketch normalization (core probe sets only) as previously described (Abdueva et al., 2007; Davicioni et al., 2006), and a variance filter was applied to eliminate genes whose standard deviation from the mean was <10 expression units of a normalized data range, leaving 7368 summarized transcripts. Differentially expressed transcripts between MCF10AT-YB1 and MCF10AT-MSCV cells in each cellular fraction were selected based on a mean fold difference of 1.5 and the associated t test, with a p value ≤ 0.05. Expression analysis was performed using the Genetrix software package (Epicenter Software).

siRNA Transfections

For transient knockdown of *YB-1* or *Snail1*, cells were transfected at ~30% confluence in 6 well plates with a Smart siRNA pool (Dharmacon)

complementary to four different regions of the corresponding mRNA or with single *YB-1* siRNAs (#1: UGACACCAAGGAAGAUGUAUU; #2: GUGAGAGUG GGGAAAAGAAUU) using the SilentFect (Bio-Rad) reagent according to the manufacturer's instructions. Concentrations of siRNAs were optimized for each cell line and are indicated in the figure legends.

Immunoblotting, Immunofluorescence, and Immunohistochemistry

Immunoblotting and immunofluorescence were performed as described previously (Sorokin et al., 2005). For origin, description, and dilutions of all antibodies used in this study see Table S3. Immunofluorescence and immunohistochemistry on formalin-fixed, paraffin-embedded tissues was performed after deparaffinization and antigen retrieval. Immunohistochemistry staining was performed using the alkaline-phosphatase-labeled streptavidin-biotin ABC kit and hematoxylin was used as a counterstain (Vector Labs). Images were acquired with an Axioplan2 fluorescence microscope (Zeiss) or confocal Nikon Eclipse TE2000-E microscope, converted to TIFF format, and arranged using Photoshop 7.0.

ACCESSION NUMBERS

Microarray data sets are available at http://www.ncbi.nlm.nih.gov/geo/ under accession code GSE13410.

SUPPLEMENTAL DATA

Supplemental Data include Supplemental Experimental Procedures, seven figures, and four tables and can be found with this article online at http://www.cell.com/cancer-cell/supplemental/S1535-6108(09)00086-5.

ACKNOWLEDGMENTS

We thank Sam Aparicio and Lena Preobrazhenskaya (BC Cancer Research Centre), Anna Krichevsky (Harvard Medical School), and Irina Groisman (University of Massachusetts Medical School) for critical reading of the manuscript; Betty Schaub, Dennis Mock, and Jonathan Buckley (Children's Hospital, Los Angeles, CA) for assistance with the Affymetrix gene expression data; and David Huntsman, Gulisa Turashvili, Torsten Nielsen, and Samuel Leung (Center for Translational and Applied Genomics) for providing breast cancer specimens. This work was supported by a grant from the Canadian Institute of Health Research (MOP62802-CIHR) to P.S. and V.E.; a ReThink Breast Cancer Career Development Award to C.E.T; and a fellowship from the Canadian Institute of Health Research, Michael Smith Foundation for Health Research, and the Royal College of Physicians Clinician Investigator Program to T.N.

Received: December 23, 2007
Revised: October 30, 2008
Accepted: March 6, 2009
Published: May 4, 2009

REFERENCES

Abdueva, D., Wing, M.R., Schaub, B., and Triche, T.J. (2007). Experimental comparison and evaluation of the Affymetrix exon and U133Plus2 GeneChip arrays. PLoS ONE *2*, e913.

Bader, A.G., and Vogt, P.K. (2005). Inhibition of protein synthesis by Y box-binding protein 1 blocks oncogenic cell transformation. Mol. Cell. Biol. *25*, 2095–2106.

Bader, A.G., and Vogt, P.K. (2007). Phosphorylation by AKT disables the anti-oncogenic activity of YB-1. Oncogene *27*, 1179–1182.

Barrallo-Gimeno, A., and Nieto, M.A. (2005). The Snail genes as inducers of cell movement and survival: implications in development and cancer. Development *132*, 3151–3161.

Beretta, L., Gingras, A.C., Svitkin, Y.V., Hall, M.N., and Sonenberg, N. (1996). Rapamycin blocks the phosphorylation of 4E-BP1 and inhibits cap-dependent initiation of translation. EMBO J. *15*, 658–664.

Bergmann, S., Royer-Pokora, B., Fietze, E., Jurchott, K., Hildebrandt, B., Trost, D., Leenders, F., Claude, J.C., Theuring, F., Bargou, R., et al. (2005). YB-1 provokes breast cancer through the induction of chromosomal instability that emerges from mitotic failure and centrosome amplification. Cancer Res. *65*, 4078–4087.

Brackstone, M., Townson, J.L., and Chambers, A.F. (2007). Tumor dormancy in breast cancer: an update. Breast Cancer Res. *9*, 208.

Cobbold, L.C., Spriggs, K.A., Haines, S.J., Dobbyn, H.C., Hayes, C., de Moor, C.H., Lilley, K.S., Bushell, M., and Willis, A.E. (2007). Identification of IRES-trans-acting factors for the Myc family of IRESs. Mol. Cell. Biol. *28*, 40–49.

Davicioni, E., Finckenstein, F.G., Shahbazian, V., Buckley, J.D., Triche, T.J., and Anderson, M.J. (2006). Identification of a PAX-FKHR gene expression signature that defines molecular classes and determines the prognosis of alveolar rhabdomyosarcomas. Cancer Res. *66*, 6936–6946.

Dawson, P.J., Wolman, S.R., Tait, L., Heppner, G.H., and Miller, F.R. (1996). MCF10AT: a model for the evolution of cancer from proliferative breast disease. Am. J. Pathol. *148*, 313–319.

Debnath, J., and Brugge, J.S. (2005). Modelling glandular epithelial cancers in three-dimensional cultures. Nat. Rev. Cancer *5*, 675–688.

Debnath, J., Muthuswamy, S.K., and Brugge, J.S. (2003). Morphogenesis and oncogenesis of MCF-10A mammary epithelial acini grown in three-dimensional basement membrane cultures. Methods *30*, 256–268.

Evdokimova, V.M., and Ovchinnikov, L.P. (1999). Translational regulation by Y-box transcription factor: involvement of the major mRNA-associated protein, p50. Int. J. Biochem. Cell Biol. *31*, 139–149.

Evdokimova, V., Ruzanov, P., Imataka, H., Raught, B., Svitkin, Y., Ovchinnikov, L.P., and Sonenberg, N. (2001). The major mRNA-associated protein YB-1 is a potent 5′ cap-dependent mRNA stabilizer. EMBO J. *20*, 5491–5502.

Evdokimova, V., Ovchinnikov, L.P., and Sorensen, P.H. (2006a). Y-box binding protein 1: providing a new angle on translational regulation. Cell Cycle *5*, 1143–1147.

Evdokimova, V., Ruzanov, P., Anglesio, M.S., Sorokin, A., Ovchinnikov, L., Buckley, J., Triche, T.J., Sonenberg, N., and Sorensen, P.H.B. (2006b). AKT-mediated YB-1 phosphorylation activates translation of silent mRNA species. Mol. Cell. Biol. *26*, 277–292.

Garcia-Gasca, A., and Spyropoulos, D.D. (2000). Differential mammary morphogenesis along the anteroposterior axis in Hoxc6 gene targeted mice. Dev. Dyn. *219*, 261–276.

Gupta, G.P., and Massagué, J. (2006). Cancer metastasis: building a framework. Cell *127*, 679–695.

Janz, M., Harbeck, N., Dettmar, P., Berger, U., Schmidt, A., Jurchott, K., Schmitt, M., and Royer, H.D. (2002). Y-box factor YB-1 predicts drug resistance and patient outcome in breast cancer independent of clinically relevant tumor biologic factors HER2, uPA and PAI-1. Int. J. Cancer *97*, 278–282.

Jimenez, J., Jang, G.M., Semler, B.L., and Waterman, M.L. (2005). An internal ribosome entry site mediates translation of lymphoid enhancer factor-1. RNA *11*, 1385–1399.

Katoh, M. (2005). WNT/PCP signaling pathway and human cancer. Oncol. Rep. *14*, 1583–1588.

Kohno, K., Izumi, H., Uchiumi, T., Ashizuka, M., and Kuwano, M. (2003). The pleiotropic functions of the Y-box-binding protein, YB-1. Bioessays *25*, 691–698.

Korsching, E., Jeffrey, S.S., Meinerz, W., Decker, T., Boecker, W., and Buerger, H. (2008). Basal carcinoma of the breast revisited: an old entity with new interpretations. J. Clin. Pathol. *61*, 553–560.

Lang, K.J., Kappel, A., and Goodall, G.J. (2002). Hypoxia-inducible factor-1alpha mRNA contains an internal ribosome entry site that allows efficient translation during normoxia and hypoxia. Mol. Biol. Cell. *13*, 1792–1801.

Lu, Z.H., Books, J.T., and Ley, T.J. (2005). YB-1 is important for late-stage embryonic development, optimal cellular stress responses, and the prevention of premature senescence. Mol. Cell. Biol. *25*, 4625–4637.

Mani, S.A., Guo, W., Liao, M.J., Eaton, E.N., Ayyanan, A., Zhou, A.Y., Brooks, M., Reinhard, F., Zhang, C.C., Shipitsin, M., et al. (2008). The

epithelial-mesenchymal transition generates cells with properties of stem cells. Cell *133*, 704–715.

Mejlvang, J., Kriajevska, M., Vandewalle, C., Chernova, T., Sayan, A.E., Berx, G., Mellon, J.K., and Tulchinsky, E. (2007). Direct repression of cyclin D1 by SIP1 attenuates cell cycle progression in cells undergoing an epithelial mesenchymal transition. Mol. Biol. Cell. *18*, 4615–4624.

Moody, S.E., Perez, D., Pan, T.C., Sarkisian, C.J., Portocarrero, C.P., Sterner, C.J., Notorfrancesco, K.L., Cardiff, R.D., and Chodosh, L.A. (2005). The transcriptional repressor Snail promotes mammary tumor recurrence. Cancer Cell *8*, 197–209.

Nelson, C.M., and Bissell, M.J. (2005). Modeling dynamic reciprocity: engineering three-dimensional culture models of breast architecture, function, and neoplastic transformation. Semin. Cancer Biol. *15*, 342–352.

Peinado, H., Quintanilla, M., and Cano, A. (2003). Transforming growth factor beta-1 induces snail transcription factor in epithelial cell lines: mechanisms for epithelial mesenchymal transitions. J. Biol. Chem. *278*, 21113–21123.

Peinado, H., Olmeda, D., and Cano, A. (2007). Snail, Zeb and bHLH factors in tumor progression: an alliance against the epithelial phenotype? Nat. Rev. Cancer *7*, 415–428.

Rae, J.M., Creighton, C.J., Meck, J.M., Haddad, B.R., and Johnson, M.D. (2007). MDA-MB-435 cells are derived from M14 melanoma cells—a loss for breast cancer, but a boon for melanoma research. Breast Cancer Res. Treat. *104*, 13–19.

Sorokin, A.V., Selyutina, A.A., Skabkin, M.A., Guryanov, S.G., Nazimov, I.V., Richard, C., Th'ng, J., Yau, J., Sorensen, P.H.B., Ovchinnikov, L.P., and Evdokimova, V. (2005). Proteasome-mediated cleavage of the Y-box binding protein 1 is linked to DNA-damage stress response. EMBO J. *24*, 3602–3612.

Stoneley, M., and Willis, A.E. (2004). Cellular internal ribosome entry segments: structures, trans-acting factors and regulation of gene expression. Oncogene *23*, 3200–3207.

Stoneley, M., Spencer, J.P., and Wright, S.C. (2001). An internal ribosome entry segment in the 5′ untranslated region of the mnt gene. Oncogene *20*, 893–897.

Stratford, A.L., Habibi, G., Astanehe, A., Jiang, H., Hu, K., Park, E., Shadeo, A., Buys, T.P., Lam, W., Pugh, T., et al. (2007). Epidermal growth factor receptor (EGFR) is transcriptionally induced by the Y-box binding protein-1 (YB-1) and can be inhibited with Iressa in basal-like breast cancer, providing a potential target for therapy. Breast Cancer Res. *9*, R61.

Sutherland, B.W., Kucab, J., Wu, J., Lee, C., Cheang, M.C., Yorida, E., Turbin, D., Dedhar, S., Nelson, C., Pollak, M., et al. (2005). AKT phosphorylates the Y-box binding protein 1 at Ser102 located in the cold shock domain and affects the anchorage-independent growth of breast cancer cells. Oncogene *24*, 4281–4292.

Thiery, J.P., and Sleeman, J.P. (2006). Complex networks orchestrate epithelial-mesenchymal transitions. Nat. Rev. Mol. Cell Biol. *7*, 131–142.

Toyo-oka, K., Bowen, T.J., Hirotsune, S., Li, Z., Jain, S., Ota, S., Escoubet-Lozach, L., Garcia-Bassets, I., Lozach, J., Rosenfeld, M.G., et al. (2006). Mnt-deficient mammary glands exhibit impaired involution and tumors with characteristics of myc overexpression. Cancer Res. *66*, 5565–5573.

Vega, S., Morales, A.V., Ocaña, O.H., Valdés, F., Fabregat, I., and Nieto, M.A. (2004). Snail blocks the cell cycle and confers resistance to cell death. Genes Dev. *18*, 1131–1143.

Yang, J., Mani, S.A., and Weinberg, R.A. (2006). Exploring a new twist on tumor metastasis. Cancer Res. *66*, 4549–4552.